Absolute measurement of total electron-impact cross sections to singlet and triplet levels in helium

John Gordon Showalter* and Richard Blair Kay
The American University, Washington, D.C. 20016
(Received 11 February 1974)

Absolute total apparent electron impact cross sections for excitation of helium $4\,^1S$, $5\,^1S$, $3\,^1P$, $4\,^1P$, $5\,^1P$, $3\,^1D$, $4\,^1D$, $5\,^1D$, $4\,^3S$, $3\,^3P$, $3\,^3D$, and $4\,^3D$ levels have been measured. The incident electron energies begin at 50 eV and extend to 500 eV for most levels studied and extend to 800 eV for the $3\,^1P$, $4\,^1S$, and $4\,^1D$ levels. The 1σ errors for most of the cross sections measured are $\pm 10\%$. The important $3\,^1P$ cross section is 15% below the Bethe approximation (Kim and Inokuti) at 200 eV and is within 6% of the Bethe approximation at 500 eV. The results are reported as polarization-corrected, apparent cross sections. Cascade-corrected cross sections are also given at selected energies. In addition the pressure dependencies of the apparent cross sections are presented for representative levels. Considerable attention is given to the description of the experimental apparatus, the treatment and analysis of the data, the techniques employed in absolute calibration, and the assessment of the errors in the experiment.

I. INTRODUCTION

This article reports the absolute measurement of total electron excitation cross sections in helium for the $4\,^1S$, $5\,^1S$, $3\,^1P$, $4\,^1P$, $5\,^1P$, $3\,^1D$, $4\,^1D$, $5\,^1D$, $4\,^3S$, $3\,^3P$, $3\,^3D$, and $4\,^3D$ levels. Monoenergetic electrons with incident energies between 50 and 800 eV were employed.

There have been many previous measurements of such cross sections, and there are several excellent review articles available.[1-4] The most comprehensive review is by Moiseiwitsch and Smith[1]; however, since its publication in 1968, several new calculations and measurements have been reported. Comparison of our results with experimental and theoretical results of others will be presented in the results section of this paper.

It suffices in this introduction to point out that there exist discrepancies and disagreements between various measurements, more so for certain levels than others. These discrepancies in some cases may be laid to poor experimental technique, or not properly taking into account the secondary mechanisms operative in the helium system.

The object in this research has been to eliminate or reduce to a minimum the experimental error. Therefore, great care has been taken in treating the effects of imprisonment, collisional transfer, impurity gases, polarization effects in the apparatus, and polarization of the optical radiation on the results. Data have been taken by photon counting under the conditions of low target densities and low beam currents. We have employed high-quality absolute pressure calibration and monitoring apparatus as well as the most accurate standard lamp obtainable in conjunction with an elaborate, well calibrated optical intensity attenuator.

The excitation functions for three of the triplet levels have been reported elsewhere,[5] but will be reproduced herein for the sake of completeness. Our absolute cross sections for these levels will be presented for the first time.

II. APPARATUS

A schematic arrangement of the experiment is shown in Fig. 1. The collision region was cylindrical about the 1-mm-diameter electron beam (Fig. 2) and was isolated from the electron gun by a 1.5-mm-diameter pumping port. The electron beam came from the gun section of a DH3-91 miniature oscilloscope tube (Fig. 3). This gun employs only electrostatic focusing and provided 15 to 40 μA beam current in the energy range from 50 to 800 eV.

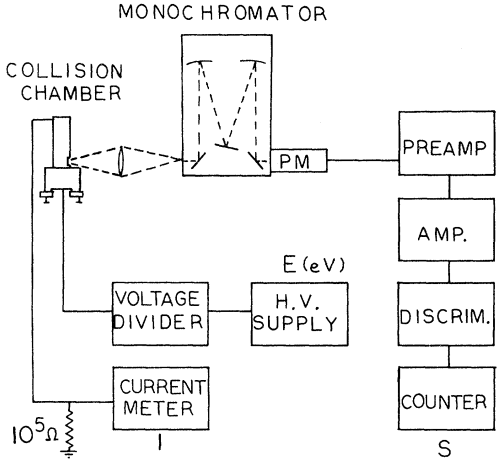

FIG. 1. Block diagram of the experimental arrangement.

Light from the collision region was detected at 90° with respect to the electron beam with an $f/7$ optical system and analyzed by a Heath EU-700 monochromator. The slits of the monochromator were oriented at right angles to the electron beam so that the slit width determined the length of beam observed. An EMI 9502B photomultiplier (PM) tube was placed at the exit slit of the monochromator. The PM tube had a very low dark noise of 30 counts/sec at room temperature.

The collision chamber was differentially pumped by an oil diffusion pump fitted with a large liquid-nitrogen cold trap. The vacuum system was constructed primarily of brass; however, limiting pressures near 10^{-7} Torr were easily achieved. The target gas was carrier grade helium which was scrubbed by a liquid-nitrogen–cooled zeolite trap prior to being flowed through the system.

The monochromator-detector system was calibrated against a GE 30A/T24/17 tungsten-ribbon-filament standard lamp.[6] This lamp was calibrated by Epply Laboratories against NBS standards of spectral radiance. The current through the lamp during calibration was held to within 0.5% of the original calibration current employed by Epply Laboratories.

A modified version of the attenuator box described by Stair *et al.*[7] (see Fig. 4) was used to reduce the relatively high intensity from the standard lamp to the low levels employed in photon counting. Diagrams and a detailed description of the attenuator box appear in the calibration section.

III. CALIBRATION

A. Pressure

The target gas pressure was constantly monitored by an MKS Baratron capacitance manometer. The Baratron was calibrated absolutely using a precision oil manometer which was constructed from an NBS design.[8] The manometer oil was "Convoil-20" and had a density of 0.8674 gm/cm^3 at 24.29 °C. The Baratron was periodically compared to the oil manometer in static calibration tests from pressures of 1000 mTorr down to 10 mTorr and was found to agree to within 1% of absolute over most of the range. The inherent linearity of the capacitance manometer was relied on for absolute pressure determination from 10 to 10^{-1} mTorr.

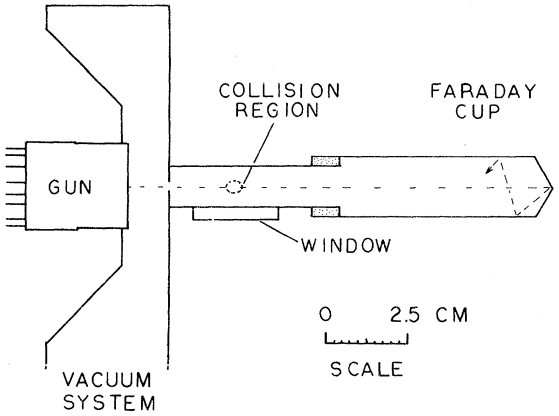

FIG. 2. Details of scattering chamber and Faraday collector.

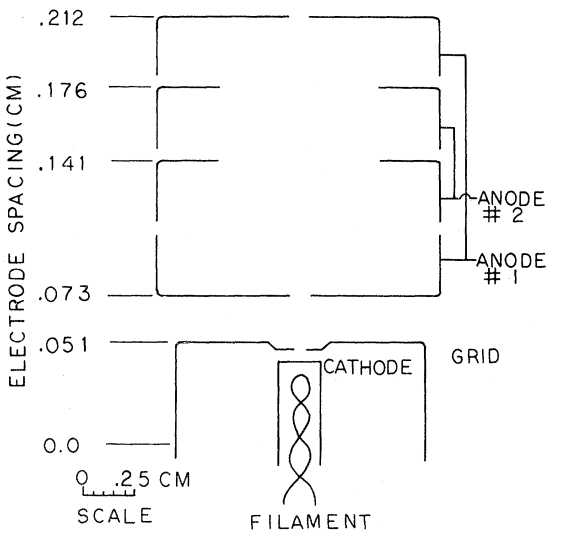

FIG. 3. Details of the electron gun: DH3-91 miniature oscilloscope tube.

B. Current

Current was monitored by measuring the voltage across a 1.00×10^5-Ω resistor with a General Radio high-impedance electrometer. The electrometer was accurate to 1% as determined by comparison with a standard source of emf.

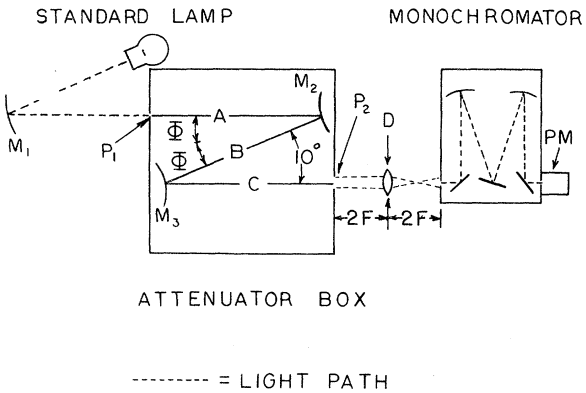

FIG. 4. Details of optical intensity calibration apparatus showing notations used in the text (Sec. III E).

C. Energy

The energy in eV of the electrons is determined by the voltage between the cathode and the chamber. This voltage was measured by a Simpson voltmeter which was in turn calibrated against a precision (0.5%) voltage divider and a General Radio high-impedence electrometer. The over-all energy of the electrons is in doubt by another 1 to 1.5 eV due to contact potentials. Retarding potential measurements indicate that the full width at half-maximum (FWHM) spread in energy at 100 eV is less than 4 eV and is probably ~0.5 eV as determined by the temperature of the indirectly heated cathode.

D. Monochromator dispersion

The linear reciprocal dispersion of the monochromator was measured for each atomic line studied and the average found to be 21.44 ± 0.48 Å/mm of slit width. The slit-width calibration was checked with a traveling microscope and found to track accurately with the dial to within 1 μm.

E. Light intensity calibration

The Heath monochromator with PM tube and associated electronics were absolutely calibrated at the end of a data run by removing the monochromator with photomultiplier from the experimental area and placing it in front of the intensity calibration setup shown in Fig. 4. Alignment pins in both positions ensured that this operation could be accomplished with little or no realignment of the associated optics.

The light attenuator was a modified version of the NBS design which has been described by Stair *et al.*[7] The polarization introduced by the attenuator box was reduced to less than 1% by using near-normal incidence ($\Phi = 5°$ in Fig. 4). The geometrical attenuation factor F_a for the box was calculated using the following expression from Stair *et al*[7]:

$$F_a = A^{-2}\left(1+\frac{B}{A}+\frac{2B\sec\Phi}{R_2}\right)^{-1}\left(1+\frac{B}{A}+\frac{2B\cos\Phi}{R_2}\right)^{-1} \times\left(1+\frac{C(R_2+2A\sec\Phi)}{B(R_2+2A\sec\Phi)+R_2A}+\frac{2C\sec\Phi}{R_3}\right)^{-1} \times\left(1+\frac{C(R_2+2A\cos\Phi)}{B(R_2+2A\cos\Phi)+R_2A}+\frac{2C\cos\Phi}{R_3}\right)^{-1}, \quad (1)$$

where A, B, C, and Φ are indicated in Fig. 4 and R_2, R_3 are the radii of curvature of mirrors M_2, M_3. The effect of the attenuator box is to transform the calibrated spectral radiance N_λ (μW/sr nm mm^2) from the standard lamp into a light intensity $H_{4\lambda}$ present across the area of the attenuator-box output aperture P_2. To calibrate at a particular wavelength, the monochromator slit width and height are imaged at the output aperture P_2 which is in effect the new source. The quantity $H_{4\lambda}$ (in W/nm mm^2) of source was computed from the expression

$$H_{4\lambda} = N_\lambda(\rho_1\rho_2\rho_3)\pi P_1^2 F_a, \quad (2)$$

where N_λ is the spectral radiance of the lamp, $(\rho_1\rho_2\rho_3)$ is the product of the reflectivities of the mirrors M_1, M_2, M_3 at a given wavelength, and πP_1^2 is the area of the box input aperture. When this spectral radiance $H_{4\lambda}$ is incident on the monochromator entrance slit of area A' and band pass ΔB (nm), the absolute light power P entering the spectrometer is

$$P = H_{4\lambda}A'\Delta B. \quad (3)$$

The number of counts/sec (S') registered by the photon counting system is proportional to this power through the proportionality factor $K(\lambda)h\nu$, i.e.,

$$S'K(\lambda)h\nu = P, \quad (4)$$

such that

$$K(\lambda) = H_{4\lambda}A'\Delta B/S'h\nu. \quad (5)$$

$K(\lambda)$ is therefore the over-all efficiency of the monochromator, photomultiplier and electronics and is the quantity determined in the calibration. The quantity $1/K(\lambda)$ has the units of counts/photon and is the over-all quantum efficiency of the system. The errors associated with the several factors comprising $K(\lambda)$ are summarized in Table I.

IV. PROCEDURE

At each data point, the signal was typically recorded for a 100-sec interval while the pressure and current were continuously monitored and held to some specific value by fine tuning the grid voltage and gas regulator needle valve.

TABLE I. Typical systematic errors in light intensity calibration. (These errors are applicable for wavelengths between 3500 and 4800 Å.)

	Estimated %	Section reference
Mirror reflectivities	5	III E
Standard lamp calibration	5	III E
Att. box input aperture area	1.6	III E
Geometrical attenuation factor	3	III E
Monochromator input slit area	1	III D
Monochromator band pass	2.4	III D
Scatter in calibration data	1	III E
Total root sum of squares	8.3	

Data were then recorded at a nearby spectral location free of helium or background gas lines, and the background count was taken for the same period of time with the same current and pressure values that were used at the center of the line of interest. This procedure was sufficient to eliminate any problems due to scattered light in the monochromator or other continuum background radiation. The capacitance-manometer zero was checked at frequent intervals during a data run, sometimes as often as every two or three 100-sec intervals at the lower pressures. The capacitance manometer was periodically absolutely calibrated against the precision oil manometer.

The electron-gun alignment was checked visually before a series of data were taken to ensure that it was centered in the scattering chamber and also that it was centered in the 1.5-mm differential pumping port. After the electron beam alignment was determined to be correct, helium was let into the chamber and the optical system was maximized by observing radiation at 5015 Å. This method gave reproducible data from day to day and month to month to within the statistics present in the photon counting method.

During the absolute calibration runs, the photon detection system was calibrated at the end of each day. Care was taken to ensure that the solid angle of the collecting optics underfilled the acceptance angle of the monochromator.

V. TREATMENT OF DATA

The apparent cross sections were determined from the relationship $Q_j' \propto S/IP$, where S is the photon signal in counts/sec, I is the current in μA, and P is the pressure in mTorr. Ideally, the gas density and current are reduced until Q_j' becomes independent of these parameters.

The beam currents employed in this experiment ranged between 1 and 40 μA and typically were 10 μA. In this current region, no nonlinearities are expected, and indeed we found all of our photon signals to vary linearly with beam currrent. However, there are strong nonlinear pressure-dependent effects in the pressure regions employed in this experiment. These are imprisonment in the $n\,^1P$ levels and the effects of collisional transfer from ^1P levels to the other levels studied. In addition, impurity gas spectra were found which could be eliminated by pressure-dependent analysis.

Finally, polarization corrections must be applied to many of the lines under study.

This section will review the steps taken in eliminating or correcting for the above. Some of these are not independent of each other at the higher pressures used in this experiment. For example the $n\,^1P$ polarization is quenched with increasing pressure due to imprisonment and collisions. However, in each correction, we extrapolate to the pressure-independent component in the measurement which is free of such effects. Therefore, it is valid to treat each correction as independent in the discussions that follow.

A. Singlet P levels and imprisonment

The ^1P levels can decay directly to the ground state emitting a resonant photon which is easily reabsorbed by a neighboring atom, an effect known as radiation trapping or imprisonment of resonance radiation. Imprisonment can be treated by adding to the excitation balance equation the fraction f_j of resonance quanta absorbed in the chamber. Phelps[9] has calculated the related quantity $g_j(p) = 1 - f_j(p)$. In the absence of cascade, Phelps relates the pressure-dependent (experimentally observed) cross section $Q_{jk}(p)$ to the absolute ^1P cross section $Q_j(p=0)$ by

$$Q_{jk}(p) = f_{jk} Q_j(p=0), \tag{6}$$

where

$$f_{jk} \equiv \frac{A_{jk}}{A + \bar{g}(p)\lambda}, \tag{7}$$

and where A_{jk} is the $j \rightharpoonup k$ transition probability, A is the sum of transition probabilities other than the resonant one from j to all lower levels, λ is the resonant transition probability, and $\bar{g}(p)$ is the average of the imprisonment factors calculated by Phelps for two limiting geometries. This average was first used by Heddle and Lucas[10] in analysis of $3\,^1P$ imprisonment and found to fit the data very well.

We fitted our data for the apparent $3\,^1P$ cross sections versus pressure by Eq. (6) at 200 eV for pressures between 0.4 and 100 mTorr. The data were fitted many times with different trial imprisonment radii, and the best fit for our particular apparatus was found to be $r_{\text{eff}} = 0.60 \pm 0.01$ cm.

It is particularly important to perform this fit at 200 eV as the $3\,^1P$ level is polarization free at 200 eV. In addition, the cascade corrections at 200 eV are approximately 2% for the optically thin case for the $3\,^1P$ level. (See, for example, Fig. 72 of Ref. 1.)

The low-pressure portions of the $4\,^1P$ and $5\,^1P$ cross sections were also found to be very well fitted by Eq. (6), using the effective imprisonment radius of 0.6 cm and the appropriate A coefficients for these levels. Further discussion of these results is given in Sec. VI.

B. Pressure nonlinearities in the excitation of $^{1,3}S$, $^{1,3}D$, and ^{3}P levels

Strongly pressure-dependent nondirect excitation of the above levels may be explained by collisional transfer from directly excited ^1P levels. A model which accounts for much of the observed transfer is due to St. John and Fowler,[11] who explained ^1P excitation function behavior in $^{1,3}D$ excitation functions by the following two-step reaction:

$$\mathrm{He}(n\,^1P)+\mathrm{He}(1\,^1S)\rightarrow \mathrm{He}(n\,^{1,3}F)+\mathrm{He}(1\,^1S),$$

$$\mathrm{He}(nF)\xrightarrow{\text{cascade}}\mathrm{He}(n'D),\quad n>n'.$$

Using the above model, Kay and Hughes have shown that the apparent cross section for a $^{1,3}D$ level fed directly by electron impact and by cascade from directly and collisionally excited F levels is expressible in the form

$$Q'(^{1,3}D)=Q_0'(^{1,3}D)[1+F^{1,3}(p)]\,, \tag{8}$$

where $Q_0'(^{1,3}D)$ is the apparent cross section to a $^{1,3}D$ level including cascade from directly excited upper states but excluding collisionally excited upper levels, and $F^{1,3}(p)$ is a complicated function of pressure which includes the collisional transfer cross sections to and from all upper $^{1,3}P$ and $^{1,3}F$ levels as well as the pressure dependence of the ^1P levels due to imprisonment.[12]

Kay and Showalter[5] have shown that for pressures below 10 mTorr for the same apparatus with an imprisonment radius of ~0.6 cm, that to first approximation $F^{1,3}(p)$ is expressible as a constant times the pressure. The constant depends on the energy dependences of the cross sections of the states involved, thus $F^{1,3}(p)\simeq C(^1P,^{1,3}D,E)p$.

For pressures below 10^{-3} Torr, the $^{1,3}D$ apparent cross sections were therefore taken to have the following form:

$$Q(^{1,3}D)=Q_0'(^{1,3}D)[1+C(^1P,^{1,3}D,E)p]\,. \tag{9}$$

As ^3D levels cascade to ^3P levels, and ^3P cascade to ^3S levels, similar but weaker nonlinearities with pressure would be expected in these levels also. Consequently, the apparent cross sections to the ^3S and ^3P levels were also taken to be of the above form, with a different constant C which depends in addition on the branching ratios from ^3D to ^3P and ^3P to ^3S levels.

Finally, the $4\,^1S$ showed some nonlinearities at low energies. It was found that $Q'(4\,^1S)$ was also fitted quite well by an expression of the same form as Eq. (9) with a different constant $C(^1S,^1P,E)$.

C. Elimination of impurity spectra

In the case of the $4\,^3S$, $3\,^1P$, and $4\,^1P$ levels, impurity spectra existed beneath the lines. The background gas density was essentially constant so that the impurity added a small constant signal to the signal/current (S/I) data. This constant was determined from S/I-vs-pressure plots which were fitted for the $4\,^3S$ transition by the following functional form:

$$\left.\frac{\mathrm{S}}{\mathrm{I}}\right|_{4^1S}=AP+BP^2+\text{impurity}\,, \tag{10}$$

where A identifies with $Q'(4\,^3\mathrm{S})$ and B with $Q'(4\,^3\mathrm{S})C(4\,^3\mathrm{S},^1P,E)$ of Sec. V C. For the $3\,^1P$ and $4\,^1P$ levels, we used the form

$$\mathrm{S/I}=Kf_{jk}P+C_{\text{impurity}}\,, \tag{11}$$

where Kf_{jk} was defined previously in Sec. V A.

In all cases, the impurity spectra produced a signal which was smaller than that due to the helium signal of interest. The error analysis for lines which were subject to impurity spectra include a component for such uncertainties.

D. Polarization corrections

Cross sections for all levels except the $^{1,3}S$ must be corrected for polarization. Previously, we have developed expressions to correct the data for the different sensitivity of the spectrometer to light polarized parallel ($I_\parallel$) and perpendicular ($I_\perp$) to the electron beam.[5] The sensitivity of the optical detection system is $S_0=C_1I_\parallel+C_2I_\perp$ where C_1 and C_2 measure the relative sensitivity and $\alpha\equiv C_1/C_2$. The polarization P is defined by

$$P=\frac{I_\parallel-I_\perp}{I_\parallel+I_\perp}\,. \tag{12}$$

We have shown[5] that the apparent cross section Q_0' is related to the uncorrected cross section measured at 90° to the beam, $Q'(90°,P,\alpha)$, by the expression

$$Q_0'=f_\alpha(P)Q'(90°,P,\alpha), \tag{13}$$

where

$$f_\alpha(P)=\frac{(\alpha+1)(1-P/3)}{2+(\alpha-1)(1-P)}\,. \tag{14}$$

Table II presents tabulations of $f_\alpha(P)$, α, and the values of P used in arriving at the polarization-corrected cross sections. The polarization data of van Raan *et al.*,[13] Heddle and Lucas,[10] and McFarland and Soltysik[14] have been employed in computing the $f_\alpha(P)$ in Table II.

The $4\,^1P$, $5\,^1P$, $3\,^1D$, $5\,^1D$ data were taken at energies associated with nearly zero polarization and required no corrections. The $4\,^1D$ apparent excitation function was corrected for polarization in the manner described by Clout and Heddle[15] by taking the data with a polaroid sheet in front of the monochromator slits with the electric field vector

TABLE II. Polarization factor $f_\alpha(P)$ and values of P and α at selected energies for the $3\,^1P \rightarrow 2\,^1S$, $3\,^3P \rightarrow 2\,^3S$, $3\,^3D \rightarrow 2\,^3P$, and $4\,^3D \rightarrow 2\,^3P$ transitions. The relative optical sensitivity α (Sec. VD) was determined experimentally while the polarization P was taken from (a) Heddle and Lucas, Ref. 10, (b) van Raan *et al.*, Ref. 13, and (c) McFarland and Soltysik, Ref. 14.

E	$3\,^1P \rightarrow 2\,^1S$ ($\alpha = 0.41$)		$3\,^3P \rightarrow 2\,^3S$ ($\alpha = 0.50$)		$3\,^3D \rightarrow 2\,^3P$ ($\alpha = 0.43$)		$4\,^3D \rightarrow 2\,^3P$ ($\alpha = 0.54$)	
(eV)	P	$f_\alpha(P)$	P	$f_\alpha(P)$	P	$f_\alpha(P)$	P	$f_\alpha(P)$
50			0.22 [a]	0.853	0.20 [a]	0.864	0.20 [a]	0.879
60			0.215 [a]	0.856	0.16 [a]	0.891	0.16 [a]	0.902
75			0.208 [a]	0.863				
100	0.33 [a]	0.777	0.185 [a]	0.875	0.03 [a]	0.979	0.03 [a]	0.980
150	0.18 [a]	0.877						
170			0.115 [a]	0.921				
200	0.08 [a]	0.942			−0.05 [c]	1.038	−0.05 [c]	1.033
300	−0.03 [b]	1.02	0.02 [a]	0.985	−0.08 [c]	1.06	−0.08 [c]	1.055
400			−0.03 [a]	1.021				
500	−0.10 [b]	1.078			−0.10 [c]	1.076	−0.10 [c]	1.069
600			−0.09 [a]	1.068				
800	−0.15 [b]	1.124						

$\vec{E}$ aligned at an angle of 54° 44′ with respect to the electron beam. This method corrects for the polarization asymmetry of the monochromator at the same time that it corrects for the asymmetrical radiation pattern.

E. Cascade corrections

The cascade corrections have been determined by the following well-known technique. Using the measured absolute apparent cross sections for the several levels measured in the experiment, approximate apparent cross sections are estimated for each higher term in a series to the $n = 15$ level by scaling the apparent cross sections by the n^{-3} law.

The cascade contribution which must be subtracted to find the cascade-free cross section for level j, being fed by cascade from level l, is then given by

$$Q_j(\text{cascade}) = \sum_{l>j}^{15} Q_l' B_{lj} ,$$

where B_{lj} is the branching ratio to level j, given by

$$B_{lj} = A_{lj} / \sum_{K<l} A_{lk} ,$$

and A_{lk} are the Einstein coefficients between levels l and k, and Q_l' the estimated apparent cross section to level l.

We chose to perform cascade corrections at selected energies where the correction is not large, and therefore not as sensitive to the use of approximate values for Q_l'.

VI. RESULTS AND CONCLUSIONS

A. The ^1P levels

Figure 5 presents the behavior of the apparent cross sections versus pressure for the $3\,^1P$, $4\,^1P$, and $5\,^1P$ levels at 200 eV. We have chosen 200 eV in this example, as the ^1P cross sections show near-zero polarization at that energy. It is seen that the Phelps-theory fit for the $3\,^1P$ level is very good, as expected, and completely accounts for the variation in the apparent cross section for more than three decades of pressure change. It is also apparent from Fig. 5 that the $4\,^1P$ and $5\,^1P$ are fitted well by the imprisonment theory for the low pressures, particularly below 10 mTorr while the high-pressure behavior departs from that predicted by the Phelps theory. This

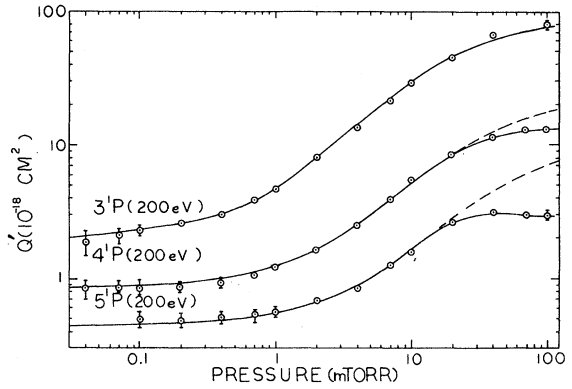

FIG. 5 Apparent cross sections versus pressure at 200 eV for the $3\,^1P$, $4\,^1P$, and $5\,^1P$ levels. The dashed lines indicate the apparent cross section in the absence of collisional transfer.

departure is because of collisional transfer from these levels as has been extensively investigated previously, particularly by the lifetime technique.[12] It should be noted that the $5\,^1P$ level shows the effects more strongly than the $4\,^1P$ level which is also in agreement with other determinations.[12,16]

The imprisonment-free cross sections for each ^1P level at each energy studied were obtained by fitting the low-pressure portion of the apparent cross section for zero effective pressure. The polarization corrections were then accounted for by the methods discussed in Sec. V.

Figure 6 presents the energy dependence of the absolute cross section for the $3\,^1P$ level as determined in this experiment, along with both the experimental and theoretical results of other workers. For energies above 100 eV, we find that our data fit the form of the Bethe asymptotic cross section (e.g., see Kim and Inokuti),[17]

$$Q_s \simeq \frac{4\pi a_0^2}{T/R}\frac{f_s}{E_s/R}\ln[C_s(T/R)]\,, \tag{15}$$

where T is the kinetic energy of the incoming electron, E_s is the excitation energy from the ground state to level s, R the Rydberg energy, a_0 the Bohr radius, f_s the generalized oscillator strength, and C_s a constant which may be related to the generalized oscillator strength. Evaluation of the slope of our data of Fig. 6, using Eq. (15), yields a generalized oscillator strength for the $3\,^1P$ level of $f_s \simeq 0.075 \pm 0.008$.

This value may be compared to the theoretical values found by Kim and Inokuti of $f_s = 0.0734$ and 0.0730 using the "length" and "velocity" formulas with Weiss wave functions[17] and values of $f_s = 0.074$ and 0.0734 found by Schiff, Pekeris, and Accad using the "length" and "velocity" formulas, respectively.[18]

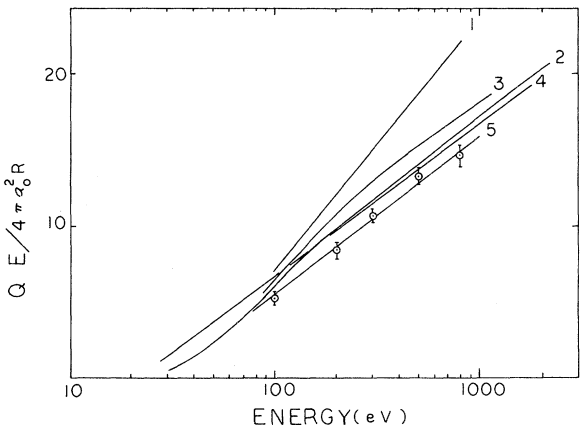

FIG. 6. Energy dependence of absolute $3\,^1P$ cross sections corrected for cascade. [St. John, Miller, and Lin (Ref. 20), curve 1; McConkey *et al.* (Ref. 21), curve 2; van Raan, de Jongh, van Eck, and Heideman (Ref. 13), curve 3; Kim and Inokuti (Ref. 17), curve 4; this work, curve 5.]

Our ^1P absolute cross sections are in very reasonable agreement with theory. The $3\,^1P$ cross section is 15% below the Bethe-approximation results of Kim and Inokuti at 200 eV and 6% below at 500 eV. Considering that our over-all experimental error is 10% for this level, the agreement is considered excellent.

The cross sections for the $4\,^1P$ and $5\,^1P$ levels were only measured at 200 eV. The $4\,^1P$ result of $(89 \pm 15)\times 10^{-20}$ cm^2 may be compared to the Bethe-approximation result of 93.4×10^{-20} cm^2 as found by Kim and Inokuti.[19]

The $5\,^1P$ cross section was measured to be $(43 \pm 8)\times 10^{-20}$ cm^2 at 200 eV. This may be compared to the estimated Born results of Bell, Kennedy, and Kingston[20] of 46.7×10^{-20} cm^2 at 200 eV. We note that in all cases for the ^1P levels, our results lie below the Born and Bethe results. This is to be expected until energies approaching 1 keV are reached. It should also be noted that the accurate first Born results of Bell, Kennedy, and Kingston for the $3\,^1P$ and $4\,^1P$ levels are in excellent agreement with the Kim and Inokuti results, there being on the order of 1% or less difference between the two theoretical results at 200 eV for the $3\,^1P$ and $4\,^1P$ levels.

The results of van Raan *et al.*,[13] McConkey *et al.*,[21] and St. John *et al.*[22] are shown for comparison in Fig. 6. The recent experimental results, including this measurement, show reasonable agreement, and are bunched around the theoretical curve. We are in best agreement with the measurement of McConkey *et al.*, for this line.

Table III presents the energy dependencies and 1σ errors for the ^1P levels as well as the other levels studied. The errors include all systematic errors listed in Table I with a summary of the over-all errors listed in Table IV. Table III also includes errors due to fitting the cross section vs pressure data to determine the pressure-independent cross sections. In the case of the $3\,^1P$ levels, for example, this fitting introduced an additional 4% error elevating the over-all error for the $3\,^1P$ cross section to around 10%.

B. The ^1S levels

The excitation of the $4\,^1S$ level was extensively studied as a function of pressure, and the results are given in Fig. 7. Also, shown in Fig. 7 is a plot of the cross sections of the $5\,^1S$ level versus pressure for the singular energy of 200 eV. It is evident that these levels are the least subject to secondary effects of all singlet levels studied and are appropriate for use as standard lines. The en-

TABLE III. Cross sections (10^{-20} cm^2).

Level	Measured absolute apparent cross sections (Beam energy in eV) 50	60	100	200	300	500	800	Cascade-corrected cross section at selected energies	Theoretical absolute cross section
$4\,^3S$	23.3±2.3	13.4±1.4	2.35±0.24	0.332±0.03	0.137±0.02	0.0372±0.004		12.4, 60 eV	9.67, 60 eV[a]
$3\,^1D$					6.47±0.72			5.94, 300 eV	3.71, 300 eV[b]
$4\,^1D$	13.3±1.3	12.4±1.2	8.20±0.80	4.01±0.40	2.84±0.28	1.59±0.16	1.05±0.10	3.97, 200 eV	2.74, 200 eV[d]
$5\,^1D$					1.52±0.17			1.45, 300 eV	1.06, 300 eV[a]
$3\,^3D$	22.4±2.5	14.1±1.6	3.10±0.34	1.18±0.13	0.91±0.30	0.62±0.25		5.90, 60 eV	0.51, 60 eV[a]
$4\,^3D$		5.19±0.60	0.81±0.09	0.095±0.03		0.036±0.020		2.69, 60 eV	0.29, 60 eV[a]
$4\,^1S$	17.3±1.7	15.6±1.6	10.6±1.1	7.00±0.70	5.42±0.54	3.77±0.38	2.40±0.24	6.58, 200 eV	8.91, 200 eV[d]
$5\,^1S$				3.0±0.4				2.78, 200 eV	4.35, 100 eV[d]
$3\,^1P$			262±26	201±20	175±18	130±14	89.7±10.	194, 200 eV	230, 200 eV[b]
$4\,^1P$				91.0±15				89.0, 200 eV	93.4, 200 eV[b]
$5\,^1P$				44.2±8				43.3, 200 eV	46.7, 200 eV[d]
$3\,^3P$	74.0±8	51.0±5	9.2±1		0.33±0.04			39.4, 60 eV	22.0, 60 eV[a]

[a]Ochkur and Bratsev, Ref. 24. [b]Kim and Inokuti, Ref. 19. [c]Kim and Inokuti, Ref. 17. [d]Bell, Kennedy, and Kingston, Ref. 20.

TABLE IV. Typical systematic errors in absolute cross-section determination. (Errors due to fitting intensity-vs-pressure curves not included.)

	Estimated %	Section reference
Solid angle definition	2	III E
Pressure-to-density and charge-to-current conversions	1	III A, B
Band pass	1	III D
Beam length	1	III D
Signal[a]	1	II
Current	1	III B
Pressure	1	III A
Light intensity calibration	8.3	Table I
Sigma (root sum of squares)	8.8	

[a]The signal strength can be measured to ~1% only for the strongest lines.

ergy dependence of the $4\,^1S$ level cross section is displayed in Fig. 8. Our absolute cross sections as well as the shape of the excitation function agree best with that of van Raan *et al.*,[13] particularly above 400 eV where our absolute values are within 10% of each other. The $1/E$ dependence predicted by the Bethe asymptotic cross section is seen to be approached at energies near 500 eV.

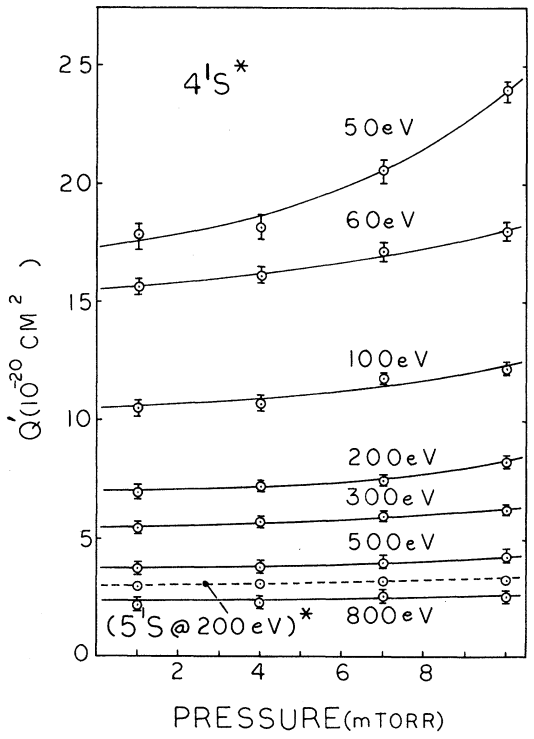

FIG. 7. Pressure variation of the apparent cross section for excitation to the $4\,^1S$ level at 50, 60, 100, 200, 300, and 800 eV and to the $5\,^1S$ level at 200 eV.

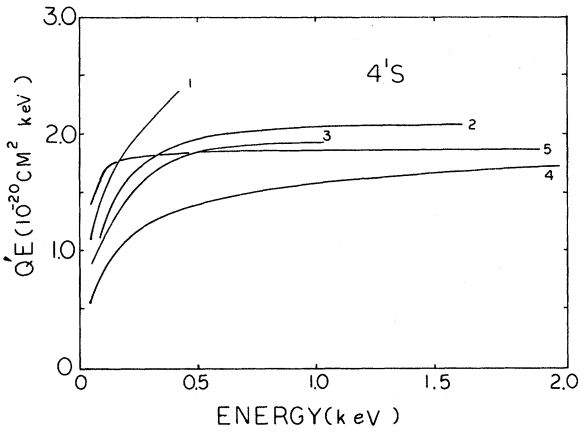

FIG. 8. Energy dependence of the apparent $4\,^1S$ cross section. [St. John, Miller, and Lin (Ref. 22), curve 1; van Raan, de Jongh, van Eck, and Heideman (Ref. 13), curve 2; this work, curve 3; Moustafa Moussa, de Heer, and Schutten (Ref. 23), curve 4; Bell, Kennedy, and Kingston (Ref. 20), curve 5, which does not include cascade.]

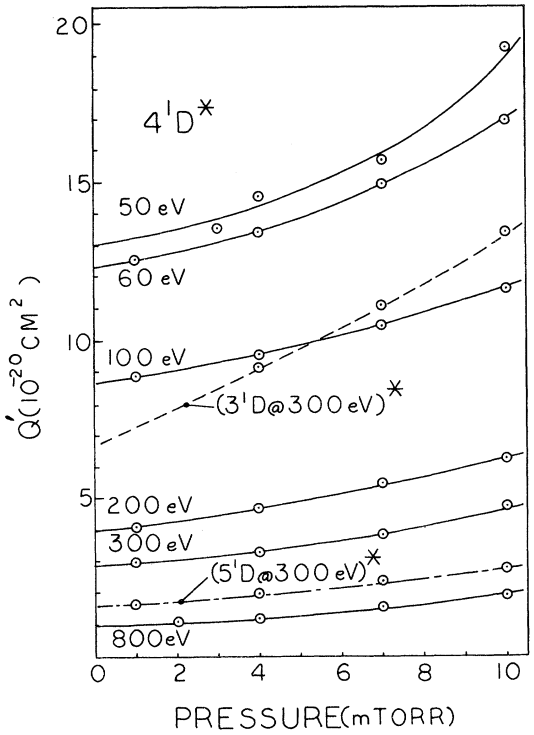

FIG. 9. Pressure variations of the apparent cross section (uncorrected for polarization) for excitation to the $4\,^1D$ level at 50, 60, 100, 200, 300, and 800 eV, to the $3\,^1D$ level at 300 eV, and to the $5\,^1D$ level at 300 eV.

Accurate Born-approximation-calculation cross sections for the $4\,^1S$ and $5\,^1S$ levels have been made by Bell *et al.*[20] Table III presents comparison to our cascade corrected results at 200 eV. The theoretical cross sections are 30 to 50% higher than the experimental values at this energy. However at higher energies, the experimental and theoretical results are closer. Our apparent $4\,^1S$ cross section at 800 eV is 2.4×10^{-20} cm^2 while the Bell *et al.* result is 2.31×10^{-20} cm^2 at this energy. Cascade corrections will be small at 800 eV, so that the experimental and theoretical results are considered in excellent agreement.

C. The ^1D levels

A complete sequence of the pressure dependencies of the apparent cross sections of the $4\,^1D$ level for energies between 50 and 800 eV is presented in Fig. 9 along with example pressure dependencies for the $3\,^1D$ and $5\,^1D$ at 300 eV. These lines are strongly pressure and polarization dependent, particularly at low energies and must be studied carefully. The derived pressure-independent absolute cross section for the $4\,^1D$ is presented in Fig. 10. [See the technique discussed in Sec. V B.] Our shape function again agrees with the Bethe asymptotic $1/E$ energy dependence; however, this dependence is found to begin at lower energies for the $4\,^1D$ than it does for the $4\,^1S$.

Recent absolute Born calculations in the Bethe representation for the $3\,^1D$ level have been carried out by Kim and Inokuti.[22] At 300 eV our $3\,^1D$ experimental value is about 70% higher than the theoretical value of Kim and Inokuti.

Bell, Kennedy, and Kingston[20] have also per-

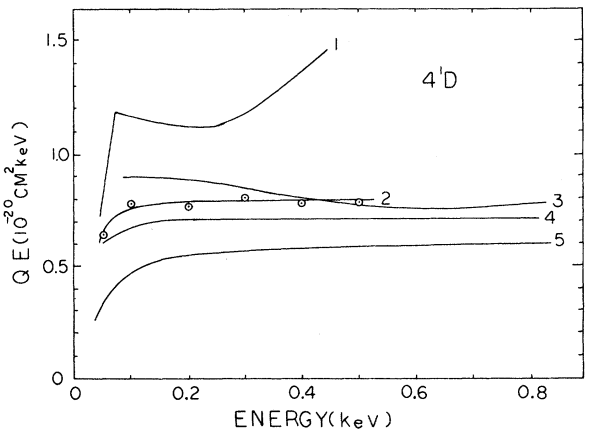

FIG. 10. Energy dependence of the apparent excitation cross sections for the $4\,^1D$ level. [St. John, Miller, and Lin (Ref. 22), curve 1; this work, curve 2; van Raan, de Jongh, van Eck, and Heideman (Ref. 13), curve 3; Moustafa Moussa, de Heer, and Schutten (Ref. 23), curve 4; Bell, Kennedy, and Kingston (Ref. 20), curve 5, which does not include cascade.]

formed accurate Born-approximation calculations for the $3\,^1D$ level, and estimated Born results for the $4\,^1D$ and $5\,^1D$ levels. Their $3\,^1D$ cross section is about 3 to 4% lower than that of Kim and Inokuti at 200 eV; however, the agreement between these two calculations is very good. Our $4\,^1D$ cascade-corrected cross section is 45% higher than the Bell *et al.* result at 200 eV, and this is a difference which does not appear to decrease with increasing energy as can be seen in Fig. 10.

The cascade-corrected $5\,^1D$ cross section at 300 eV is also found to lie about 40% above the results of Bell *et al.*[20]

Our experimental results again agree most favorably with those of van Raan *et al.*, as can be seen in Fig. 10. Also shown in Fig. 10 are the results of St. John *et al.*[22] and Moustafa Moussa, de Herr, and Schutten.[23]

D. The triplet levels

As mentioned earlier, we have reported previously on the excitation function and pressure dependencies of the $4\,^3S$, $3\,^3P$, and $3\,^3D$ levels.[5] Figure 11 presents the absolute apparent cross sections versus energy for these levels. We have found that the $4\,^3S$ level is free from any excitation showing nonexchange energy dependence; i.e. we find the cross section to this level decreases as $(1/E)^{3\pm0.2}$, in agreement with the Ochkur approximation.[23]

We did find a departure from a fast monotonic decrease of cross section with energy for other triplet levels. The $3\,^3D$ cross section shows what can be interpreted as two energy dependencies; one associated with exchange excitation which is dominant at low energies and drops rapidly with energy; and one which falls off roughly as $1/E$ which we attributed to cascade from mixed $^{1,3}F$ levels. The ^1F level cross sections would be expected from the Bethe approximation to show a $1/E$ energy dependence. This dependence also seemed to be showing up in the high-energy portion of the $3\,^3P$ cross section and was attributed to cascade from the $1/E$ portion of n^3D cross sections. We have now measured the apparent cross section for the $4\,^3D$ level, and find a much smaller portion of $1/E$ component than in the $3\,^3D$ level (see Fig. 12). The difference in the relative amount of $1/E$ component is very difficult to explain on the basis of mixed F-level cascade, and may be due to transfer from higher, mixed angular-momentum levels.

The comparison of absolute theoretical cross sections to absolute experimental cross sections is very difficult in the case of the triplet system. At the low energies, where signals are strong, i.e. where cross sections are high, the experimental values are very accurate. However, theoretical results are not accurate until higher energies are reached.

We have chosen to perform cascade corrections on the apparent cross sections at the lower energies where we are confident that the direct exchange excitation of these levels is dominant, i.e. at 60 eV, the lower energy regime in this experiment. Table III presents our cascade-corrected absolute cross sections at 60 eV, and also the theoretical cross sections of Ochkur and Bratsev.[24]

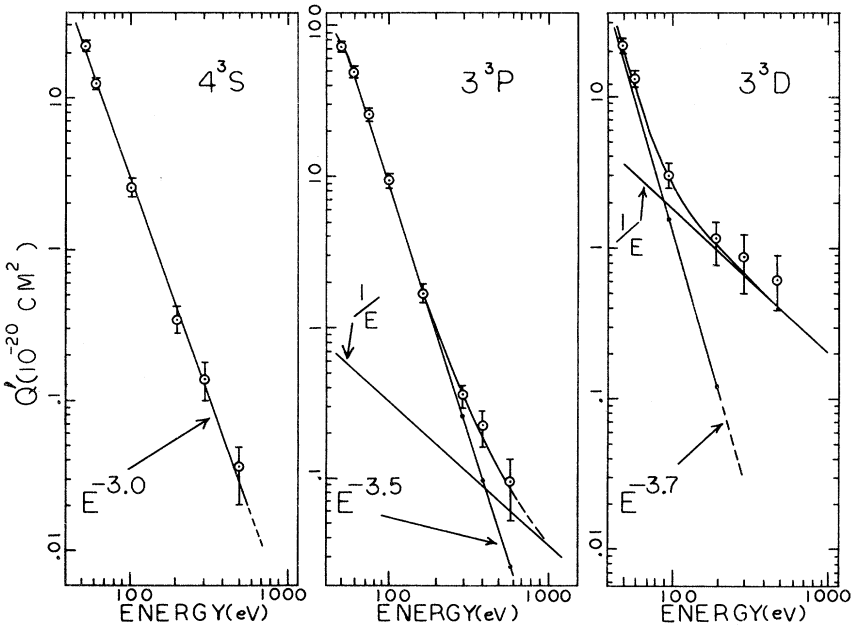

FIG. 11. Absolute apparent excitation functions of triplet levels at zero effective pressure. (a) $4\,^3S$: No slow component present up to 500 eV. Slope of resultant curve is -3.0 ± 0.2. (b) $3\,^3P$: Subtraction of indicated slower $1/E$ component yields a resultant curve with a slope of -3.5 ± 0.2. (c) $3\,^3D$: Subtraction of indicated slower $1/E$ component yields a resultant curve with a slope of -3.7 ± 0.5.

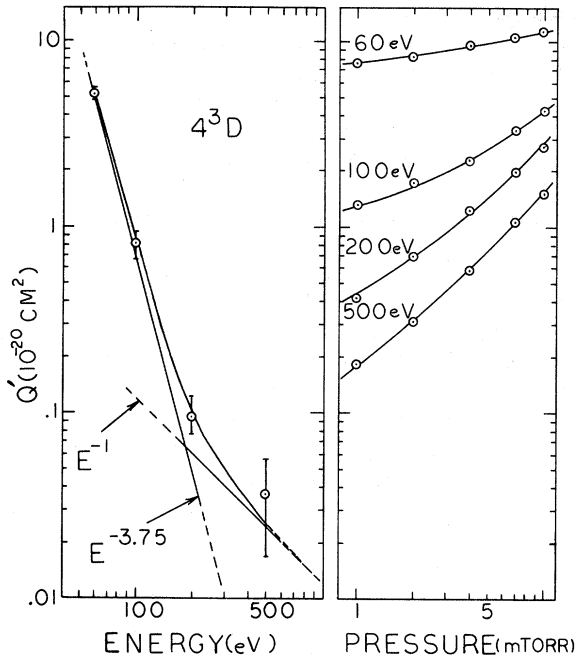

FIG. 12. (a) Absolute apparent excitation function at zero effective pressure for the $4\,^3D$ level. Subtraction of indicated slower $1/E$ component yields a resultant curve with a slope of -3.75 ± 0.05. (b) The pressure variation of the $4\,^3D$ apparent cross sections (uncorrected for polarization at 60, 100, 200, and 500 eV.)

The experimental $4\,^3S$ cross section is about 27% higher than the Ochkur result, and the experimental $3\,^3P$ cross section is about 30% higher than the Ochkur results at 60 eV. While this agreement must be considered as marginal, the results for the ^3D levels are much worse.

The experimental $3\,^3D$ and $4\,^3D$ cross sections are roughly a factor of 10 greater than the theoretical calculations at 60 eV. It should be noted that the $3\,^3D$ apparent cross section has been reduced by a little over 50%. This is very unusual in that most cascade corrections at these energies are in the neighborhood of 20%. However, the work of Anderson, Hughes, and Norton has shown that a little over half of the $3\,^3D$ *non-pressure-dependent* excitation comes from the 4^3F level.[25]

We can also compare our absolute triplet cross sections with experimental results of other workers. Table V presents our results and those of van Raan *et al.* and St. John *et al.* at 60 eV.

It is difficult to understand how our results can be so close to those of van Raan *et al.* for the singlet system and so different in the triplet system, where our apparent cross sections are generally a factor of 2 higher. Our results agree better with the older results of St. John at these energies.

TABLE V. Apparent absolute cross sections at 60 eV (units of 10^{-20} cm^2).

Level	This work	van Raan *et al.*[a] (Ref. 13)	St. John *et al.*[b] (Ref. 11)
$4\,^3S$	13.4	5.84–7.43	10.5
$3\,^3P$	51.0	26.7–24.4	53.0
$3\,^3D$	14.1		17
$4\,^3D$	5.2		4.7

[a] Results for two different apparatuses.
[b] Cascade corrections applied.

It should be noted, however, that St. John's results are known to be in error at higher energies.

E. Conclusions

Great difficulties are encountered in measuring absolute cross sections which require the simultaneous absolute determination of photon emission rate, ground-state density of the target gas, and beam current and energy. Experimental errors (1σ) are found to be seldom better than 10%, often to be about 20%. With such limitations in mind, the following generalizations can be made.

1. Singlet system: Energies above 100 eV

Good agreement between recent experimental measurements and theory is found for ^1P level excitation, particularly above 500 eV, where for example this experiment is 6% below the Bethe-approximation results of Kim and Inokuti. The experimental results of McConkey *et al.* are 3% below and van Raan *et al.* 12% above those of Kim and Inokuti at this energy.

Good agreement is also found between recent experimental results and theory for ^1S levels. This is to be expected experimentally, as the ^1S levels are the least subject to the secondary problem of collisional transfer and there are no polarization corrections for ^1S states. It is also apparent that the Born approximation is more accurate for excitation to the low-angular-momentum levels.

Reasonable agreement is also found between recent experimental measurements for ^1D levels. However, our results lie about 70% above the Bethe-approximation results for the $3\,^1D$ level. The recent experimental results for the $4\,^1D$ and $5\,^1D$ levels lie about 40 to 45% above the Born-approximation results of Bell *et al.*[10]

2. Triplet system

There still exist wide discrepancies between experimental results in the case of triplet-system cross sections. We believe our shape functions are the most accurate measured to data. The absolute accuracy of our cross sections should be

no worse than 20%; however, our results disagree with those of van Raan *et al.* by considerably more than this.

Our results and theory show reasonable agreement (30%) for the $4\,^3S$ level excitation. Reasonable agreement can also be argued for the $3\,^3P$ level on the basis of the results of van Raan *et al.* but not on the basis of ours. However, in the case of ^3D excitation, there seems to be a factor of 10 discrepancy between experiment and theory which can not be laid to experimental error. It would appear that the exchange-excitation approximation underestimates higher-angular-momentum levels, the more so the higher the angular momentum of the level involved.

ACKNOWLEDGMENTS

The authors wish to acknowledge many beneficial discussions with Dr. C. Kuyatt, of the National Bureau of Standards, and also with Dr. G. Chamberlain, now at the Joint Institute for Laboratory Astrophysics. In addition we wish to thank Dr. Kuyatt for providing us with accurately measured manometer oil used in the pressure calibration for the experiment.

---

*Now with the Naval Research Laboratory, Washington, D. C. 20390.

[1]B. L. Moiseiwitsch and S. J. Smith, Rev. Mod. Phys. 40, 238 (1968).

[2]W. S. Fite, in *Atomic and Molecular Processes*, edited by D. R. Bates (Academic, New York, 1962).

[3]D. W. O. Heddle and R. G. W. Kessing, in *Advances in Atomic and Molecular Physics*, edited by D. R. Bates and I. Esterman (Academic, New York, 1968), Vol. 4.

[4]M. S. W. Massey and E. M. S. Burhop, *Electronic and Ionic Impact Phenomena, Vol. 1: Collisions of Electrons with Atoms* (Oxford U. P., London, 1969).

[5]R. B. Kay and J. G. Showalter, Phys. Rev. A 3, 1998 (1971).

[6]*Precision Measurement and Calibration*, edited by H. K. Hammond III and H. L. Mason, NBS Spec. Publ. No. 300 (U. S. GPO, Washington, D. C., 1971), Vol. 7.

[7]R. Stair, W. B. Fussell, and W. E. Schneider, Appl. Opt. 4, 85 (1965).

[8]A. M. Thomas and J. L. Cross, J. Vac. Sci. Technol. 4, 1 (1967).

[9]A. V. Phelps, Phys. Rev. 110, 1362 (1958).

[10]D. W. O. Heddle and C. B. Lucas, Proc. R. Soc. Lond. A271, 129 (1963).

[11]R. M. St. John and R. G. Fowler, Phys. Rev. 122, 1813 (1961).

[12]R. B. Kay and R. H. Hughes, Phys. Rev. 154, 61 (1967).

[13]A. F. J. van Raan, J. P. de Jongh, J. van Eck, and H. G. M. Heideman, Physics (N. Y.) 53, 45 (1971).

[14]R. H. McFarland and E. A. Soltysik, Phys. Rev. 128, 1758 (1962).

[15]P. N. Clout and D. W. O. Heddle, J. Opt. Soc. Am. 59, 715 (1969).

[16]J. D. Jobe and R. M. St. John, Phys. Rev. A 5, 295 (1972).

[17]Y. K. Kim and M. Inokuti, Phys. Rev. 175, 176 (1968).

[18]B. Schiff, C. L. Pekeris, and Y. Accad, Phys. Rev. A 4, 885 (1971).

[19]Y. K. Kim and M. Inokuti, Phys. Rev. 184, 38 (1969).

[20]K. L. Bell, D. J. Kennedy, and A. E. Kingston, J. Phys. B 2, 26 (1969).

[21]J. W. McConkey, F. G. Donaldson, and M. A. Hender, Phys. Rev. Lett. 26, 1413 (1971); and F. G. Donaldson, M. A. Hender, and J. W. McConkey, J. Phys. B 5, 1192 (1972).

[22]R. M. St. John, F. L. Miller, and C. C. Lin, Phys. Rev. 134, A888 (1964).

[23]H. R. Moustafa Moussa, F. J. de Heer, and J. Schutten, Physica 40, 517 (1969).

[24]V. I. Ochkur and V. F. Bratsev, Opt. Spektrosk. 19, 490 (1965) [Opt. Spectrosc. 19, 274 (1965)].

[25]R. J. Anderson, R. H. Hughes, and T. G. Norton, Phys. Rev. 181, 198 (1969).